

Dynamic finite-size scaling at first-order transitions

Andrea Pelissetto

Dipartimento di Fisica dell'Università di Roma "La Sapienza" and INFN, Sezione di Roma I, I-00185 Roma, Italy

Ettore Vicari

Dipartimento di Fisica dell'Università di Pisa and INFN, Sezione di Pisa, I-56127 Pisa, Italy

(Dated: October 27, 2018)

We investigate the dynamic behavior of finite-size systems close to a first-order transition (FOT). We develop a dynamic finite-size scaling (DFSS) theory for the dynamic behavior in the coexistence region where different phases coexist. It is characterized by an exponentially large time scale related to the tunneling between the two phases. We show that, when considering time scales of the order of the tunneling time, the dynamic behavior can be described by a two-state coarse-grained dynamics. This allows us to obtain exact predictions for the dynamical scaling functions. To test the general DFSS theory at FOTs, we consider the two-dimensional Ising model in the low-temperature phase, where the external magnetic field drives a FOT, and the 20-state Potts model, which undergoes a thermal FOT. Numerical results for a purely relaxational dynamics fully confirm the general theory.

PACS numbers: 05.70.Fh, 64.70.qj, 64.60.an, 05.50.+q

I. INTRODUCTION

Close to a phase transition point finite-size systems exhibit a universal finite-size scaling (FSS) behavior [1–7], which characterizes both static and dynamic equilibrium properties. FSS is also observed in out-of-equilibrium phenomena, for instance, in the quenching of a random configuration at the critical point. In general, it is observed when the size L of the system is larger than any microscopic length scale and if the observation time t is comparable with the time scale $\tau(L)$ of the slowest critical mode, which generally diverges in the infinite-volume limit [8]. At continuous transitions the finite-size behavior is characterized by power laws, with universal critical exponents which only depend on a few global features of the system; see, e.g., Refs. [9, 10]. A universal FSS is also observed at first-order transitions (FOTs) [11–20]. In this case one observes power-law behaviors with simple exponents, which are closely related to the space dimension of the system.

At FOTs, dynamic phenomena play a very important role, due to the presence of very slow modes with large time scales. Indeed, in the absence of continuous symmetries, any local dynamics is very slow, due to an exponentially large tunneling time between the two phases coexisting at the transition point: $\tau(L) \sim \exp(\sigma L^{d-1})$ for a system of size L^d , where the constant σ is generally related to the interface free energy. Also the dynamic behavior, both in equilibrium and out-of-equilibrium conditions, is supposed to show universal features and, in particular, to exhibit a universal dynamic FSS (DFSS). A satisfactory understanding of the DFSS properties of the system close to a FOT is important for experiments on relatively small systems, when the longest time scale of the system is of the order of the time scale of the experiment.

In this paper we consider the evolution of a finite-size system close to a FOT. We focus on the interplay between

the finite size of the system and the distance (in parameter space) from the FOT point. We show that several large-scale quantities obey DFSS laws, analogous to those holding at continuous transitions, the only difference being that the time scale $\tau(L)$ increases exponentially with L . Moreover, as long as the control parameters (for instance, temperature, magnetic field, ...) are such the system is always in the coexistence region, the observed behavior can be interpreted in terms of a generic Markov two-state coarse-grained dynamics. Using such dynamics, we can derive exact predictions for the DFSS functions. To test the general DFSS theory, we present numerical analyses of the two-dimensional (2D) Ising model in the low-temperature phase—here the external magnetic field drives a FOT—and of the 2D 20-state Potts model, which undergoes a thermal FOT. Some related issues are investigated in Refs. [21, 22], where the off-equilibrium behavior observed when some parameter is slowly varied across a FOT (the analogue of the Kibble-Zurek dynamics at a continuous transition [23, 24]) is investigated.

The paper is organized as follows. In Sec. II we consider the two-dimensional Ising model, define the relevant observables, and the dynamics we consider. The general scaling theory is developed in Sec. III and tested in Sec. IV. In Sec. V we discuss a different type of finite-size scaling that allows us to investigate the single-droplet region. In Sec. VI we extend the general discussion to the case in which the magnetic field does not vanish only on a subset of lattice points. In Sections VII, VIII, IX, X we extend the discussion to the Potts model. In Sec. XI we summarize and draw our conclusions. In the Appendix A we report the computation of the average magnetization for an Ising model in which the magnetic field is nonvanishing only in a single site. In App. B we compute the average energy for the Potts model at the transition in the presence of a single strongly ferromagnetic bond.

II. THE ISING CASE: DEFINITIONS

A. The model

We consider the 2D Ising model defined on a square $L \times L$ lattice in the presence of an external magnetic field. Its Hamiltonian is

$$H = - \sum_{\langle ij \rangle} s_i s_j - h \sum_i s_i, \quad (1)$$

where $s_i = -1, 1$ and the first sum is over all nearest-neighbor pairs i, j . The model undergoes a paramagnetic-ferromagnetic transition for $h = 0$ and $T = T_c$, with [25]

$$\beta_c = \frac{1}{2} \ln(1 + \sqrt{2}), \quad T_c = 1/\beta_c. \quad (2)$$

For $T < T_c$ and $h \rightarrow 0$ the system is spontaneously magnetized in the thermodynamic limit. The spontaneous magnetization per site is given by

$$m_0(T) = [1 - \sinh(2\beta)^{-4}]^{1/8}. \quad (3)$$

In the following we also need the interface tension κ , which is also known exactly [26]:

$$\kappa = 2 + \ln[\tanh(\beta)]/\beta. \quad (4)$$

In a finite square box of linear size L , the behavior of the system depends on the boundary conditions. For boundary conditions that preserve the \mathbb{Z}_2 inversion symmetry, for instance, for periodic boundary conditions (PBC), the magnetization vanishes for $h = 0$. For small values of h , static FSS holds in terms of the scaling variable

$$r_1 = hL^2. \quad (5)$$

This means that an appropriate universal behavior is observed when taking the limits $h \rightarrow 0$, $L \rightarrow \infty$ at fixed r_1 . In particular, in the FSS limit the magnetization per site m becomes

$$m = m_0 f_{\text{eq}}(r_1), \quad f_{\text{eq}}(r_1) = \tanh(\beta m_0 r_1). \quad (6)$$

Note that $m \neq |m_0|$ for any finite r_1 , indicating that both free-energy minima contribute to equilibrium properties, i.e., that the system is always in the coexistence region.

B. The dynamics

We consider a relaxational dynamics at fixed $T < T_c$ and fixed magnetic field h . We use three different implementations of the Metropolis algorithm, which, as we shall see, all show the same dynamical behavior. In most of the simulations we use the checkerboard update. If (n_x, n_y) , $0 \leq n_x, n_y < L$, are the coordinates of the lattice sites, we first update all spins at points such that

$n_x + n_y$ is even (the order is irrelevant since they do not interact), then all spins at points such that $n_x + n_y$ is odd. We also consider a sequential update, in which we first sequentially update all spins on the line $n_y = 0$, then those on the line $n_y = 1$, and so on. Finally, we consider the random update, in which spins are randomly chosen. All times are measured in sweeps. In the checkerboard and sequential updates, a sweep consists in a Metropolis update attempt of all spins. In the random case, it consists in L^2 random update attempts. In all cases, we start the dynamics from a completely ordered configuration with $s_i = -1$ for all i 's.

The main purpose of the paper is that of verifying the existence of a DFSS behavior, which extends the static FSS to the dynamics when h is small and $T < T_c$. As the relevant scaling variable is expected to be $r_1 = hL^2$, simulations are performed at fixed T and r_1 for different values of L , varying at the same time the magnetic field as $h = r_1/L^2$. Note that $h \rightarrow 0$ as L increases.

In the evolution we measure the average magnetization per site

$$M(t) = \frac{1}{L^2} \sum_i s_i, \quad (7)$$

where t is the time, and the corresponding average renormalized magnetization

$$m_r(t, r_1, L) = \frac{1}{m_0} \langle M(t) \rangle, \quad (8)$$

where the average is over the different dynamic histories and we have not reported explicitly the temperature dependence. Moreover, given a number μ satisfying $-1 < \mu < 1$, we define the first-passage time $t_f(\mu)$ as the smallest time such that

$$M[t_f(\mu)] = \mu m_0. \quad (9)$$

We can then consider its average

$$T_f(\mu, r_1, L) = \langle t_f(\mu) \rangle, \quad (10)$$

and its probability distribution

$$P(x, r_1, L) = \left\langle \delta \left(\frac{t_f(\mu)}{T_f(\mu, r_1, L)} - x \right) \right\rangle. \quad (11)$$

III. THE ISING CASE: DYNAMIC SCALING BEHAVIOR IN THE COEXISTENCE REGION

A. General arguments

Close to the FOT at $h = 0$ and $T < T_c$, physical observables show a scaling behavior in terms of h and of the size of the system L , which depends in general on the boundary conditions. For PBC, the only case we consider in this work, static observables show FSS once they are expressed in terms of $r_1 = hL^2$. To extend FSS to the

dynamic case, it is necessary to identify the appropriate time scale of the dynamics. As we consider the large- L limit at fixed r_1 , the system is always in the coexistence region. Therefore, the relevant time scale is the one that controls the large-time dynamic behavior for $h = 0$.

For symmetric boundary conditions, in the low-temperature phase the largest autocorrelation times are associated with flips of the magnetization. This should occur by means of the generation of configurations characterized by two coexisting phases separated by two approximately planar interfaces. Their probability is of the order of $\exp(-\sigma L)$, where

$$\sigma = 2\beta\kappa, \quad (12)$$

and κ is the planar interface tension. The factor of two is due to the presence of two interfaces, which are necessarily present because of the PBC. Standard arguments [27] allow us to predict that the time needed to observe a reversal of the magnetization is proportional to $\exp(\sigma L)$ with power corrections. Therefore, we define a time scale

$$\tau(L) = L^\alpha \exp(\sigma L), \quad (13)$$

where α is an appropriate exponent.

Note that Eq. (13) assumes that the relevant mechanism for the generation of the opposite phase is the creation of strip-like domains parallel to the lattice axes and not the creation of spherical droplets, as it has already been checked for $h = 0$, see Ref. [28]. This reflects the fact that spherical droplets are unstable. Indeed, at $h \simeq 0$ (in the FSS limit h scales as L^{-2}) they tend to shrink due to their curvature, taking a time $t \sim R^2$, where R is their size [29]. Equivalently, one can note that a critical droplet has a size R_c of the order of [30] a/h , so that $R_c/L = aL/r_1$. Therefore, at fixed r_1 we find $R_c \gg L$, confirming the irrelevance of the droplets in the limit we are considering here.

Once we have identified the correct time scale, we can introduce the scaling variables that parametrize the dynamics. Beside the static quantity r_1 , we define

$$r_2 = t/\tau(L). \quad (14)$$

Then, we expect

$$\begin{aligned} m_r(t, r_1, L) &\approx f_m(r_1, r_2), \\ T_f(\mu, r_1, L) &\approx \tau(L) f_T(r_1, \mu), \\ P(x, r_1, L) &\approx f_P(r_1, x). \end{aligned} \quad (15)$$

B. Coarse-grained flip dynamics

The above scaling relations define several scaling functions. We now show that they can be exactly predicted. Let us consider the dynamics of a single system. At $t = 0$ the magnetization $M(t)$ is equal to -1 . As t increases, $M(t)$ rapidly changes and, after a few iterations, we observe that $M(t) \approx -m_0$, with fluctuations

that decrease as L increases. Then, suddenly, the magnetization changes sign. In a very short time interval Δt , with $\Delta t \ll \tau(L)$, $M(t)$ increases and $M(t) \approx +m_0$ at the end. Then, the magnetization remains constant for a long time interval and then, again, in a very short time interval Δt , we observe the reversal of the magnetization, obtaining $M(t) \approx -m_0$. This flipping process continues as t increases, guaranteeing that the time average of $m(t)$ converges to the value given in Eq. (6) as the run length goes to ∞ .

Since on time scales of the order of $\tau(L)$ the reversal of the sign of the magnetization is essentially instantaneous, we can consider a simpler coarse-grained dynamics. First, we assume that $M(t)$ takes only two values, $\pm m_0$. Second, as we expect the dynamics restricted within each free-energy minimum to be rapidly mixing, we can assume that the coarse-grained dynamics is Markovian. Under these conditions, the dynamics is completely parametrized by the rates I_+ and I_- defined by

$$\begin{aligned} P[M(t) = -m_0 \rightarrow M(t + dt) = +m_0] &= I_+ dt, \\ P[M(t) = +m_0 \rightarrow M(t + dt) = -m_0] &= I_- dt, \end{aligned} \quad (16)$$

where $P(\cdot)$ is the probability of the considered transition.

Consider now N_{tot} different dynamic histories and let $N_+(t)$ be the number of systems for which $M(t) = +m_0$ at time t . Then, we can write

$$dN_+(t) = -N_+(t)I_- dt + [N_{\text{tot}} - N_+(t)]I_+ dt. \quad (17)$$

If we define $n(t) = N_+(t)/N_{\text{tot}}$ we obtain the equation

$$\frac{dn}{dt} = -nI_- + (1 - n)I_+. \quad (18)$$

Since $n(t = 0) = 0$, the solution is

$$n(t) = \frac{I_+}{\lambda} (1 - e^{-\lambda t}), \quad \lambda = I_+ + I_-. \quad (19)$$

Then, since $m_r(t) = 2n(t) - 1$, we obtain

$$m_r(t) = \frac{I_+ - I_-}{\lambda} - \frac{2I_+}{\lambda} e^{-\lambda t}. \quad (20)$$

For large t we must recover the equilibrium value (6), which implies

$$\frac{I_-}{I_+} = e^{-2\beta m_0 r_1}. \quad (21)$$

Finally, the rate I_+ can be related to the first-passage time. Indeed, first note that, if the dynamics consists in essentially instantaneous flips, the quantity $T_f(\mu, r_1, L)$ is expected to become independent of μ in the scaling limit, i.e., we can simply write $T_f(\mu, r_1, L) \approx \tau_f(r_1, L)$. Then, since the probability that the first flip of the magnetization from $-m_0$ to $+m_0$ occurs in the time interval $[t, t + dt]$ is $\exp(-I_+ t)I_+ dt$, in the scaling limit we have

$$\frac{1}{I_+} = \tau_f(r_1, L) \quad (22)$$

and

$$P(x, r_1, L) = e^{-x}. \quad (23)$$

Relations (21) and (22) allow us to rewrite $m_r(t)$ as

$$m_r(t) \approx f_{\text{eq}}(r_1) - [1 + f_{\text{eq}}(r_1)]e^{-t/T_i}, \quad (24)$$

$$T_i = \frac{\tau_f(r_1, L)}{1 + e^{-2\beta m_0 r_1}},$$

where $f_{\text{eq}}(r_1)$ is the equilibrium FSS function (6). In the scaling limit we expect that

$$\tau_f(r_1, L) = \tau(L)f_T(r_1), \quad (25)$$

see Eq. (15), and therefore $m_r(t)$ becomes a universal function of r_1 and r_2 .

Note that all predictions are independent of the sign of h and also hold when $h < 0$, i.e., when the magnetic field does not favor the flip of the magnetization. The symmetry of the model under $h \rightarrow -h$ implies $I_+(-h) = I_-(h)$ and therefore the relation

$$\frac{\tau_f(r_1, L)}{\tau_f(-r_1, L)} = \frac{g_\tau(r_1)}{g_\tau(-r_1)} = e^{-2\beta m_0 r_1}. \quad (26)$$

IV. THE ISING CASE: MONTE CARLO RESULTS IN THE COEXISTENCE REGION

To verify the previous predictions, we perform Monte Carlo simulations for $T = 0.9T_c$ and several values of r_1 , ranging from -1 to 50 . All data reported in this section are obtained by using the checkerboard update, except in the last subsection, where we compare our results for the three different updates.

A. Testing the coarse-grained flip dynamics

As a first test, we verify that $T_f(\mu, r_1, L)$ becomes independent of μ for $L \rightarrow \infty$, cf. Eq. (22). We consider the ratio

$$R_T(\mu, r_1, L) = \frac{T_f(\mu, r_1, L)}{T_f(0.9, r_1, L)}. \quad (27)$$

Such a quantity is plotted in Fig. 1 for $r_1 = -1, 10, 50$. There are clearly two regimes. For μ negative and close to -1 , the ratio is small. For these values of μ , $T_f(\mu, r_1, L)$ simply gives the typical timescale of the fluctuations of the magnetization within the free-energy minimum with $m_r \approx -1$, which is the stable one for $r_1 = -1$, and the metastable one for the other two values of r_1 . Then, $T_f(\mu, r_1, L)$ becomes essentially constant, which indicates that these values of the magnetization are only reached in the very rapid process in which the magnetization changes sign. As L increases, $R_T(\mu, r_1, L)$ starts to be 1 at decreasing values of μ , a consequence of the decrease of the fluctuations of the average magnetization

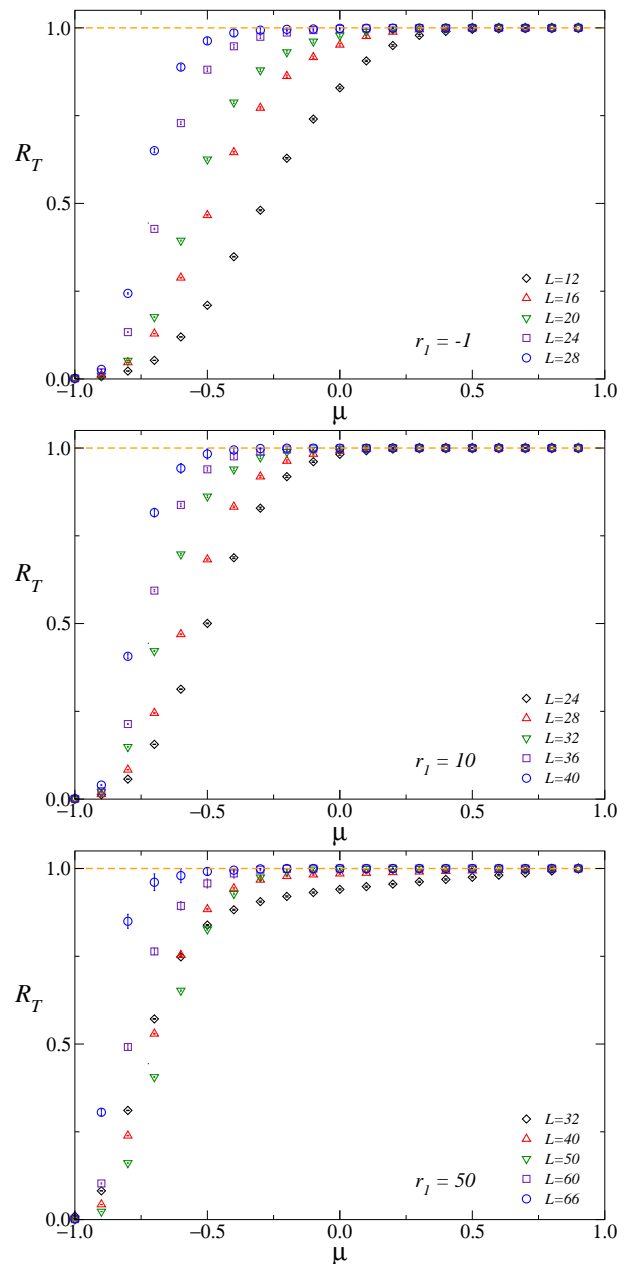


FIG. 1: (Color online) Ratio $R_T(\mu, r_1, L)$ for $r_1 = -1, 10, 50$ and several values of L , as a function of μ . Here $T = 0.9T_c$.

with the volume. For $L \rightarrow \infty$ it is then natural to expect $R_T(\mu, r_1, L) = 1$ for any $\mu > -1$. It is interesting to observe that the size corrections increase significantly with r_1 . For $r_1 = -1$, the ratio at $\mu = 0$ is essentially 1 for $L \gtrsim 24$, while one should take $L \gtrsim 40$ for $r_1 = 50$.

The numerical data provide also information on the nature of the size corrections. For this purpose we fit $[1 - R_T(\mu, r_1, L)]$ at fixed μ and r_1 to aL^{-p} . If we use the data for $r_1 = 10$ ($24 \leq L \leq 40$) we obtain $p = 5.3(2)$, $5.9(5)$, $6.9(1.0)$, $7.3(1.3)$ for $\mu = -0.3, -0.2, -0.1, 0$, respectively. Similarly large powers are obtained if one considers other values of r_1 . The very large values obtained

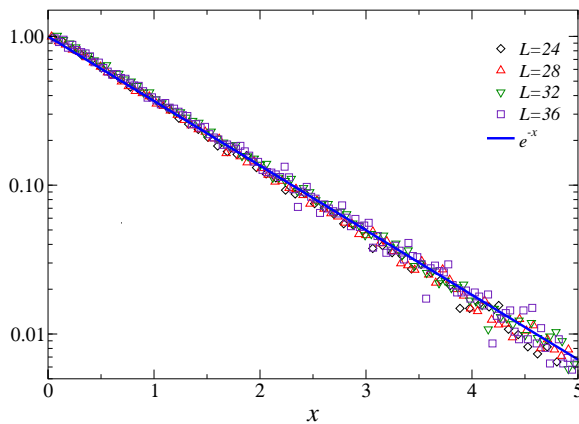


FIG. 2: (Color online) Distribution function of the first passage time as a function of $x = t_f(0.9)/T_f(0.9, r_1, L)$ for $r_1 = 10$, $T = 0.9T_c$, and several values of L . The thick blue line corresponds to e^{-x} .

for p make a power behavior rather unlikely. We have also tried to parametrize the scaling corrections as ae^{-bL} . For $r_1 = 10$ we obtain $b = 0.25(5)$, $0.25(3)$, $0.22(2)$, $0.20(1)$, for the same values of μ as before. The χ^2 is slightly better than that obtained in the power-law fit, which makes the exponential convergence more plausible than the power-law behavior. It is interesting to note that the prefactor b appears to be independent of r_1 , within errors (say, within 10-15%). For instance, for $\mu = -0.2$ we obtain $b = 0.233(5)$ for $r_1 = -1$ ($L \geq 12$) and $b = 0.20(2)$ for $r_1 = 50$ ($L \geq 40$).

As a second test of the general theory, we verify the relation (26) by comparing the results for $r_1 = 1$ and $r_1 = -1$. We consider the quantity

$$R_2(L) = \frac{T_f(0.9, r_1, L)}{T_f(0.9, -r_1, L)} e^{2\beta m_0 r_1} \quad (28)$$

for $r_1 = 1$. We obtain $R_2(L) = 0.998(4)$, $0.996(4)$, $1.008(5)$, $1.016(8)$, $0.987(14)$, for $L = 12, 16, 20, 24, 28$, respectively. Therefore, the data confirm the general relation (28).

We also check the predictions for the distribution function $P(x, r_1, L)$. Results for $r_1 = 10$ are reported in Fig. 2 together with the theoretical prediction. Data follow the expected exponential behavior quite precisely, confirming the two-level nature of the dynamics.

As a last test of the general theory, we verify prediction (24) for the renormalized magnetization. As we have verified the independence of $T_f(\mu, r_1, L)$ on μ , we take $T_f(0.9, r_1, L)$ as time scale. In Fig. 3 we report results for $r_1 = -1, 1, 10, 50$ and several values of L . We observe an excellent scaling behavior: data corresponding to different box sizes fall on top of each other quite precisely. In Fig. 3 we also report the prediction (24) (thick lines). It falls on top of the numerical data, confirming the general coarse-grained picture of the dynamics.

r_1	Range	χ^2/DOF	a	α
4.9	[20,36]	3.5/2	0.411(7)	0.1(2)
	[24,36]	3.4/1	0.407(14)	1.0(4)
	[20,36]	30/3	σ	1.61(1)
	[24,36]	7.3/2	σ	1.70(2)
	[28,36]	5.8/1	σ	1.74(4)
10	[24,40]	5.2/2	0.428(6)	0.8(2)
	[28,40]	0.1/1	0.401(13)	0.9(4)
	[24,40]	82/3	σ	1.56(1)
	[28,40]	2.8/2	σ	1.73(2)
	[32,40]	0.1/1	σ	1.79(4)

TABLE I: Results of fits to Eq. (29) and to Eq. (30) (here we set $a = \sigma = 0.379028\dots$) for two values of r_1 . Here $\mu = 0.9$ and $T = 0.9T_c$. “Range” gives the interval of sizes L considered in the fit, χ^2 is the sum of the residuals and DOF is the number of degrees of freedom of the fit.

B. The time scale of the dynamics

In Sec. III A we have performed a careful test of the dynamics using the first-passage time as the time scale. This allows us to compare theoretical predictions and numerical data without the need of tuning any parameter. Here we wish to check the size dependence of time scale, verifying Eq. (13). Using Eqs. (22) and (25), we fit the data of $T_f(\mu = 0.9, r_1, L)$ for $r_1 = 4.9$ and $r_1 = 10$ to the ansatz

$$\log T_f(\mu = 0.9, r_1, L) = aL + \alpha \ln L + b. \quad (29)$$

If Eq. (13) holds, we should find $a = \sigma$, with $\sigma \approx 0.379028$ for $T = 0.9T_c$, the temperature value of our runs. The results of the fits are reported in Table I (first two rows for each value of r_1). We observe that the results, both for a and α , are significantly size dependent, so it is difficult to quote a reliable estimate. In any case the estimates of a apparently approach σ as smaller L results are discarded. Given also the somewhat large statistical error, results appear to be substantially consistent with the prediction $a = \sigma$. Then, assuming $a = \sigma$, we can obtain a more precise estimate of α , by fitting the data to

$$\log[T_f(\mu, r_1, L)e^{-\sigma L}] = \alpha \ln L + b. \quad (30)$$

The estimates of α are reported in Table I. Again, we observe a trend with the size L of the systems: as L increases also α increases. Clearly, there are significant corrections to scaling, as also indicated by the large values of the χ^2/DOF (DOF is the number of the degrees of freedom of the fit). It is difficult to quote a final result as data show an increasing trend with the minimal size used in the fit. Conservatively, we quote $\alpha \approx 2$. Our result is consistent with the result of Ref. [28] that studied the heat-bath dynamics at $h = 0$, finding $\alpha \approx 2.14$ on smaller lattices $L \leq 16$.

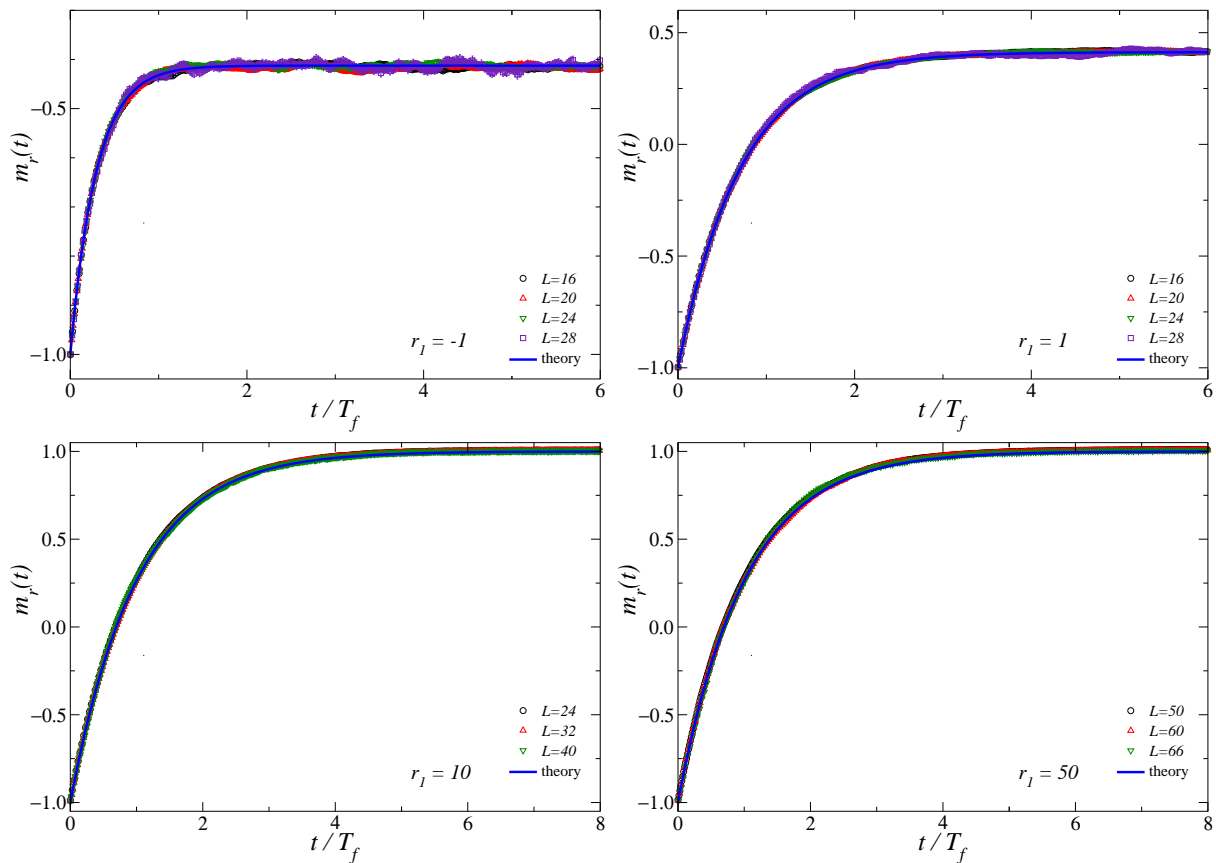


FIG. 3: (Color online) Renormalized magnetization $m_r(t)$ versus $t/T_f(0.9, r_1, L)$. Top left: $r_1 = -1$; top right: $r_1 = 1$; bottom left: $r_1 = 10$; bottom right: $r_1 = 50$. The thick line going through the points is the theoretical prediction (24). In all cases $T = 0.9T_c$.

C. Different dynamics

Up to now we have only reported results for the checkerboard dynamics. We wish now to discuss the dynamic behavior observed when using the sequential and the random dynamics. For this purpose, we have performed runs with these two different update types at $T = 0.9T_c$, $r_1 = 10$, and $L = 24, 28, 32$. As before, we analyze the time dependence of the renormalized magnetization. For both dynamics, we verify Eq. (24) for the renormalized magnetization, confirming the universality of the spin-flip dynamics. We can then compare the efficiency of the different updating procedures, measuring the ratio

$$S_{\text{dyn}}(r_1, L) = \frac{T_{f,\text{dyn}}(0.9, r_1, L)}{T_{f,\text{checker}}(0.9, r_1, L)}, \quad (31)$$

where “dyn” refers to the sequential and random updates. For the first type of update we obtain $S_{\text{seq}}(r_1, L) = 0.983(5), 0.995(5), 0.992(6)$, for $L = 24, 28, 32$, respectively, and $r_1 = 10$. The sequential update is essentially equivalent to the checkerboard one. For the random update we obtain instead $S_{\text{random}}(r_1, L) = 4.41(2), 4.48(3), 4.53(5)$, for $L =$

24, 28, 32, respectively. The random update is clearly slower, but the difference is only a factor of 4.5. Note that the time scale of the different updates differs only by a multiplicative constant. This is at variance with what happens outside the coexistence region, in which droplets dominate [30] (see also Sec. V).

V. THE SINGLE-DROPLET REGION

In the previous sections we have considered the dynamic FSS in the coexistence region. In that case, one is considering the effective equilibrium dynamics that consists in flips between the two essentially degenerate free-energy minima. The relevant phenomenon is the generation of strip-like domains, while droplet generation does not play any role. In this section we consider instead the intermediate regime in which the phase change can occur either through strip-like domains or by means of the growth of a droplet. Since the relevant time scales are proportional to $e^{\sigma L}$ and $e^{a/h}$, respectively, this regime can be probed by considering the scaling limit $h \rightarrow 0$, $L \rightarrow \infty$ at fixed

$$s = hL. \quad (32)$$

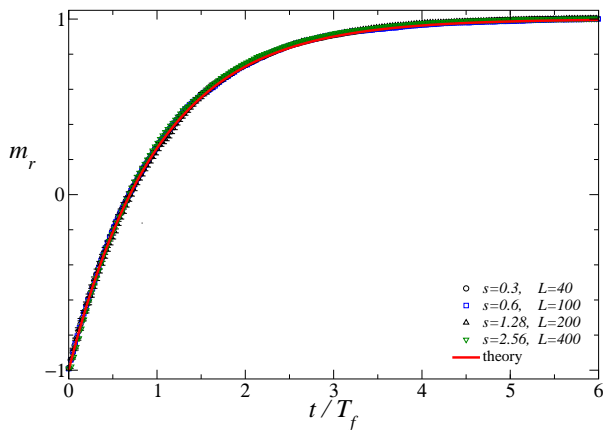


FIG. 4: (Color online) Renormalized magnetization $m_r(t)$ versus $t/T_f(0.9, s, L)$. We report data for different values of $s = hL$; for each of them the lattice size L is chosen so that data are in the asymptotic scaling regime. The thick line going through the points is the theoretical prediction (33). In all cases $T = 0.9T_c$.

In this limit $r_1 \rightarrow \infty$ and therefore, for $h > 0$, in equilibrium we have $m \approx +m_0$: if we start from configurations with $m = -1$, we only observe a single flip to the phase with positive magnetization. This off-equilibrium dynamics can be described as discussed in Sec. III B, taking simply $L_- = 0$. All expressions simplify and we obtain, e.g.,

$$m_r(t) = 1 - 2 \exp[-t/\tau_f(s, L)] \quad (33)$$

for any value of s . While scaling functions are supposed to be independent of s , any time scale should have a nontrivial s dependence. For instance, we expect

$$T_f(\mu, s, L) \sim L^\alpha \exp[A(s)L]. \quad (34)$$

For the values of s in which the magnetization flip occurs through the generation of strip-like domains, we should have $A(s) = \sigma$, while in the regime in which droplets dominate we should find $A(s) \sim 1/s$. Moreover, also α should depend on the regime one is considering. In particular, Ref. ([30]) predicts $\alpha \approx 0$ in the single-droplet region for the sequential update and $\alpha = 1$ for the random update [31]. As before, we expect the results to be independent of μ in the scaling limit.

To verify the predicted behavior, we have performed simulations for $s = 0.3, 0.6, 1.28, 2.56$ at $T = 0.9T_c$. For each value of s we consider a few values of L to verify that the size of the system is large enough to allow us to observe the scaling asymptotic regime. Results for $m_r(t)$ are reported in Fig. 4. As expected, all data fall on top of each other and are consistent with the theoretical prediction (33).

We have also studied the behavior of the first-passage time, which becomes μ independent as L increases. As before, we use the data at $\mu = 0.9$ to analyze the L and s dependence of the time scale. Our data are not

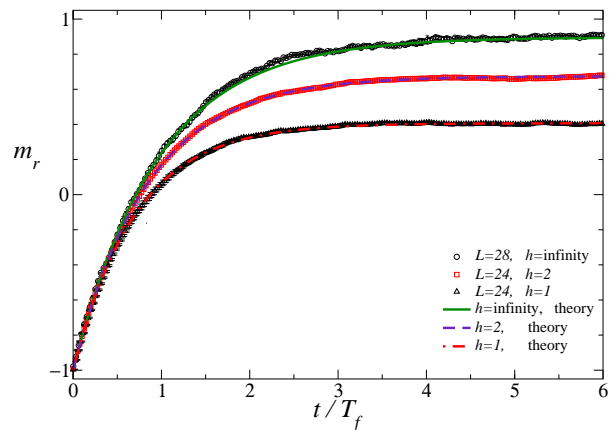


FIG. 5: (Color online) Renormalized magnetization $m_r(t)$ versus $t/T_f(0.9, h, L)$. We report data for different values of the magnetic field h on a single site; for each of them the lattice size L is chosen so that data are in the asymptotic scaling regime. The thick lines going through the points are the theoretical prediction (37). In all cases $T = 0.9T_c$.

precise enough and not sufficiently numerous to allow us to estimate the exponent α . For this reason we have performed two fits, considering

$$\ln[T_f(0.9, s, L)L^{-\alpha}] = a + A(s)L, \quad (35)$$

fixing $\alpha = 0$ (the droplet-region prediction if we assume the equivalence of the sequential and of the checkerboard update) and 2 (coexistence-region prediction). We obtain $A(s) = 0.238, 0.114, 0.053, 0.025$ for $\alpha = 0$ and $s = 0.3, 0.6, 1.28$, and 2.56 , respectively. For the same values of s and for $\alpha = 2$ we have $A(s) = 0.161, 0.091, 0.042, 0.019$. Statistical errors are significantly smaller than 10^{-3} . Note that all results satisfy the approximate scaling $A(s) \sim 1/s$, indicating that for these values of s droplet formation is the relevant mechanism. It is also interesting to note that the χ^2 of the fit is significantly smaller for $\alpha = 0$ than for $\alpha = 2$, in agreement with the general results of Ref. [30] on the exponent α .

VI. THE ISING MODEL WITH A MAGNETIC FIELD ON A SMALL LATTICE DOMAIN

It is also interesting to study the dynamics when one considers a magnetic field that is present only on a small subset of sites. Specifically, we consider again Hamiltonian (1), replacing the magnetic term $h \sum_i s_i$ with $\sum_i h_i s_i$. We consider here two cases: (i) the magnetic field is present only on a single site, that is h_i is always zero except at a single lattice point; (ii) h_i is nonvanishing only on a lattice line.

A. Magnetic field on a site

In the low-temperature phase the addition of a magnetic field on a single lattice point is enough to break the \mathbb{Z}_2 invariance of the model, thereby generating a finite magnetization. A simple calculation gives, see App. A,

$$m_r = \hat{f}_{\text{eq}}(h) = m_0 \tanh \beta h. \quad (36)$$

Note that for any value of h , the absolute value of $|m_r|$ is always less than 1, so that the system is always in the crossover region. The arguments of Sec. III B should then apply for any h . Taking into account the different expression for the equilibrium magnetization, we obtain

$$m_r(t) = \hat{f}_{\text{eq}}(h) - [1 + \hat{f}_{\text{eq}}(h)]e^{-t/T_s}, \quad (37)$$

$$T_s = \frac{1}{2}\tau_f(h, L) \left[1 + \hat{f}_{\text{eq}}(h)\right].$$

In Fig. 5 we show the results for $m_r(t)$ for $h = 1, 2, \infty$. Scaling holds and results are perfectly consistent with Eq. (37). We have also verified that $T_f(\mu, h, L)$ is independent of μ and scales as in the case of a uniform magnetic field at fixed r_1 . We consider the ratio

$$R(h, L) = \frac{T_f(0.9, h, L)}{T_f(0.9, r_1 = 1, L)}, \quad (38)$$

where $T_f(0.9, r_1 = 1, L)$ is the first-passage time for a uniform magnetic field with $r_1 = hL^2 = 1$. We obtain for $h = \infty$ $R(h, L) = 0.175(1), 0.175(1), 0.174(1), 0.176(4)$ for $L = 16, 20, 24, 28$, respectively. For $h = 1$ we obtain analogously $R(h, L) = 0.929(4), 0.911(4), 0.930(8)$, for $L = 16, 20, 24$. The ratio is independent of L , indicating that the first-passage time scales identically in the two cases.

B. Magnetic field on a line

We now consider the case in which the magnetic field is nonvanishing only on a lattice line, for instance, on all lattice points (x, y) such that $y = 1$. It turns out that the relevant scaling variable is

$$u_1 = hL. \quad (39)$$

As L increases, the estimates of $m_r(t)$ at fixed u_1 fall onto a single scaling curve. Moreover, we verify that the equilibrium value of the magnetization is still given by Eq. (6) with u_1 replacing r_1 . The general discussion of Sec. III B applies also to this case and indeed, the results for $m_r(t)$ are consistent with Eq. (24) by simply replacing r_1 with u_1 , see Fig. 6.

We have also investigated the L dependence of the first-passage time, considering the ratio

$$R(u_1, L) = \frac{T_f(0.9, u_1, L)}{T_f(0.9, r_1, L)}, \quad (40)$$

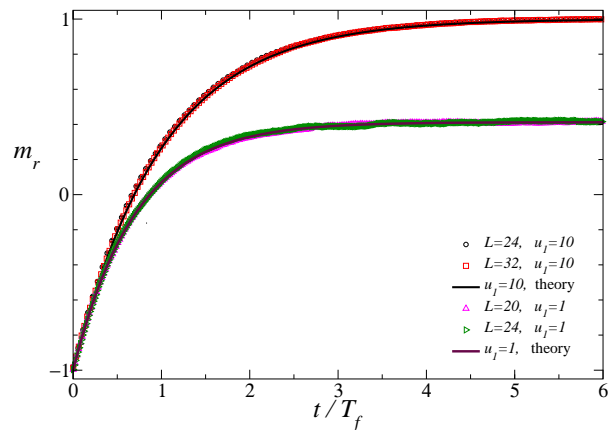


FIG. 6: (Color online) Renormalized magnetization $m_r(t)$ versus $t/T_f(0.9, u_1, L)$. We report data for different values of L and of $u_1 = hL$, where h is nonvanishing only on a lattice line. The thick lines going through the points are the theoretical predictions. In all cases $T = 0.9T_c$.

between the first passage time for the case of a magnetic field on a line and that for a uniform field. We always take $u_1 = r_1$, so that the compared systems have the same equilibrium value of the magnetization. For $u_1 = r_1 = 10$, we find $R(u_1, L) = 0.140(1), 0.125(1), 0.113(1)$ for $L = 24, 28, 32$, respectively, while for $u_1 = r_1 = 1$ we have $R(u_1, L) = 0.975(6), 0.960(8)$ for $L = 20, 24$. The ratio apparently decreases with L . A fit of the data with $u_1 = r_1 = 10$ gives $R(u_1, L) \sim L^{-\beta}$, $\beta = 0.75(10)$. This indicates that, at fixed $u_1 = r_1$, i.e., for the same equilibrium value of the magnetization, the dynamics is faster when h is nonvanishing only on one line than for a uniform magnetic field.

VII. THE POTTS CASE: DEFINITIONS

To test whether the observed behavior in the Ising case is generic, i.e., it is typical of any FOT, we study a second model that shows a thermal, i.e., temperature-driven, FOT. We consider the 2D q -state Potts model on a square lattice. Its Hamiltonian reads

$$H = - \sum_{\langle xy \rangle} \delta(s_x, s_y), \quad (41)$$

where the sum is over the nearest-neighbor sites of a square lattice, s_x (*color*) are integer variables $1 \leq s_x \leq q$, $\delta(a, b) = 1$ if $a = b$ and zero otherwise. It undergoes a phase transition [32, 33] at

$$\beta_c = \ln(1 + \sqrt{q}), \quad T_c = 1/\beta_c. \quad (42)$$

The transition is of first order for $q > 4$. We consider $L \times L$ square lattices with periodic boundary conditions (PBC), which preserve the q -permutation symmetry. In infinite volume the energy density $E = \langle H \rangle / L^2$ is discontinuous at T_c , with different $E_c^\pm \equiv E(T_c^\pm)$. We define a

renormalized energy density

$$E_r \equiv \Delta_e^{-1} (E - E_c^-), \quad \Delta_e \equiv E_c^+ - E_c^-, \quad (43)$$

which satisfies $E_r = 0, 1$ for $T \rightarrow T_c^-$ and $T \rightarrow T_c^+$, respectively.

Close to the transition, the system shows FSS in terms of the scaling variable

$$r_1 = L^d \delta, \quad \delta \equiv \beta/\beta_c - 1. \quad (44)$$

In this limit the finite-size energy density scales as [21]

$$E_r(T, L) \approx \mathcal{E}_{\text{eq}}(r_1) = (1 + q e^X)^{-1} \quad (45)$$

with $X = \Delta_e \beta_c r_1$.

In the following we focus on the case $q = 20$, for which [32] $E(T_c^+) = -0.626530\dots$, $E(T_c^-) = -1.820584\dots$ We will also be interested in the interface tension, which takes the value [34–36] $\beta_c \kappa = 0.185494\dots$ for $q = 20$.

We consider a heat-bath dynamics at fixed $T < T_c$. We use the checkerboard update and we start the dynamics from a fully disordered configuration. In the evolution we measure the energy $H(t)$, which allows us to define the average renormalized energy, using Eq. (43) and defining $E = \langle H \rangle / L^2$. As we use PBC the magnetization

$$M_k = \frac{1}{L^2} \left\langle \sum_{\mathbf{x}} \mu_k(\mathbf{x}) \right\rangle, \quad \mu_k(\mathbf{x}) \equiv \frac{q \delta(s_{\mathbf{x}}, k) - 1}{q - 1}, \quad (46)$$

vanishes for any value of T . To investigate the magnetic properties we consider

$$I_G = L^{-2} \sum_{k=1}^q \sum_{\mathbf{x}, \mathbf{y}} \langle \mu_k(\mathbf{x}) \mu_k(\mathbf{y}) \rangle. \quad (47)$$

In the infinite-volume limit and for $T < T_c$, we have

$$I_G = \frac{q L^2 m_0^2}{q - 1}, \quad (48)$$

where m_0 is the spontaneous magnetization, which can be defined by introducing an infinitesimal breaking of the q state symmetry. For $q = 20$, we have [32, 33] $m_0 = 0.941175\dots$

VIII. THE POTTS CASE: SCALING ARGUMENTS

The scaling arguments presented for the Ising case extend without changes to the Potts transition. As before, we define a time scale

$$\tau(L) = L^\alpha \exp(\sigma L) \quad (49)$$

so that, in the FSS limit, the dynamics in a finite volume can be parametrized by using r_1 and $r_2 = t/\tau(L)$ as scaling variables.

Also in the Potts case we can perform the coarse graining of the dynamics. Indeed, we can assume that the system starts in the high- T phase and then it suddenly jumps in any of the equivalent q magnetized states. Therefore, Eq. (18) holds, provided we identify $n(t)$ as the fraction of magnetized systems at time t . Since $\mathcal{E}_r(t) = 1 - n(t)$, we obtain

$$\mathcal{E}_r(t) = \frac{I_-}{\lambda} + \frac{I_+}{\lambda} e^{-\lambda t}, \quad (50)$$

with $\lambda = I_+ + I_-$. For $t \rightarrow \infty$ we should recover Eq. (45), which implies

$$\frac{I_-}{I_+} = \frac{1}{q} e^{-\beta_c \Delta_e r_1} \quad (51)$$

It follows

$$\mathcal{E}_r(t) = \mathcal{E}_{\text{eq}}(r_1) + \frac{q}{q + e^{-\beta_c \Delta_e r_1}} e^{-t/T_p}, \quad (52)$$

$$T_p = \frac{q}{I_+ (q + e^{-\beta_c \Delta_e r_1})}. \quad (53)$$

The quantity I_G can be predicted as well. In the coarse-grained dynamics the combination

$$I_{Gr}(t) = \frac{q - 1}{q m_0^2 L^2} I_G(t) \quad (54)$$

is equivalent to $1 - \mathcal{E}_r$, so that

$$I_{Gr} = \frac{q}{q + e^{-\beta_c \Delta_e r_1}} \left(1 - e^{-t/T_p} \right). \quad (55)$$

IX. THE POTTS CASE: MONTE CARLO RESULTS

To test the general theory, we perform Monte Carlo simulations for four different values of r_1 , $r_1 = 1/16, 1/4, 1, 4$, respectively, varying the system size L from 12 to 40. As a first test, we verify Eq. (52), considering the quantity

$$\tilde{E}(t) = \frac{1}{q} e^{-\beta_c \Delta_e r_1} \left[(1 + q e^{\beta_c \Delta_e r_1}) \mathcal{E}_r - 1 \right]. \quad (56)$$

According to Eq. (52), it should behave as a pure exponential, i.e., $\tilde{E}(t) = e^{-t/T_p}$, in the scaling limit. Data accurately satisfy this behavior.

We then fit the data to $\log \tilde{E} = a t$, obtaining estimates of T_p . In Fig. 7 we report the data of $E_r(t)$ as a function of t/T_p and compare them with the theoretical prediction (52). We observe perfect scaling: data fall on top of each other for different values of L and are fully consistent with Eq. (52). Very good scaling is also observed for $I_G(t)$. Data behave in full agreement with Eq. (55).

Finally, we verify the size dependence of the scale, performing the same fits as we did in the Ising case. We consider the time scale T_p and first perform fits to Eq. (29).

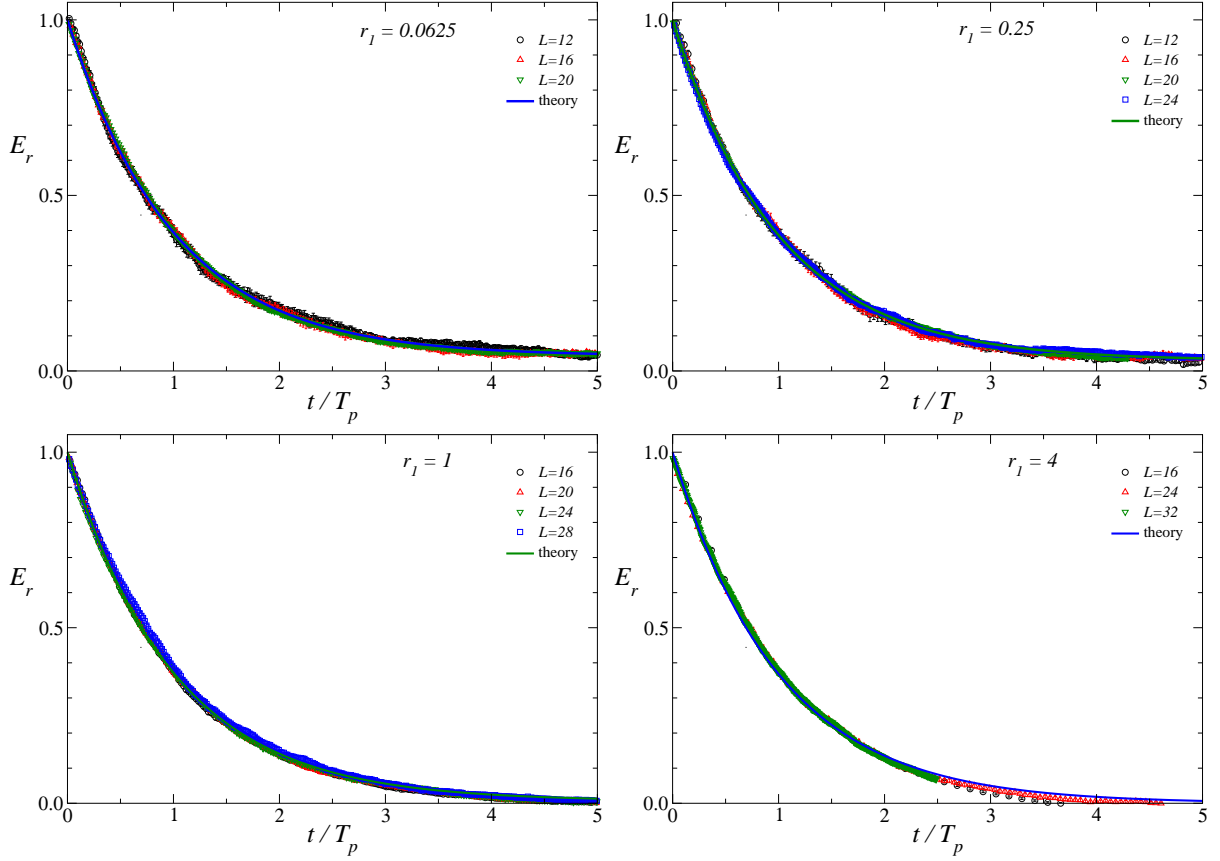


FIG. 7: Estimates of E_r versus t/T_p for $r_1 = 0.065$ (top left), 0.25 (top right), 1 (bottom left), 4 (bottom right), for several values of L . The thick line in each panel is the theoretical prediction (52).

TABLE II: Results of fits of T_p to Eq. (29) and to Eq. (30) (here we set $a = \sigma = 0.370988\dots$) for different values of r_1 . “Range” gives the interval of sizes L considered in the fit.

r_1	range	a	α
0.25	[12,24]	0.38(2)	1.4(3)
	[12,24]	σ	1.54(2)
1.0	[16,32]	0.37(3)	1.5(6)
	[20,32]	0.32(6)	2.7(1.4)
	[16,32]	σ	1.56(4)
	[20,32]	σ	1.58(6)
	[24,32]	σ	1.34(13)
4.0	[16,40]	0.41(2)	0.0(5)
	[20,40]	0.39(3)	0.6(8)
	[16,40]	σ	0.96(9)
	[20,40]	σ	1.07(9)
	[24,40]	σ	1.16(14)
	[28,40]	σ	1.26(18)

Results are reported in Table II. For all values of r_1 the constant a is consistent with $\sigma = 2\beta\kappa \approx 0.371$, confirming the theoretical prediction (49). To estimate α , we perform fits to Eq. (30), using the theoretical prediction

for σ . For $r_1 \approx 0.25$ and 1, results give $\alpha \approx 1.5$. Results for $r_1 = 4$ are also consistent: the estimates of α are lower, but show a significant increasing trend.

X. POTTS MODEL: SCALING IN THE PRESENCE OF A SINGLE STRONGLY FERROMAGNETIC BOND

The analysis we have presented in Sec. VI for the Ising model with a magnetic field different from zero only on a subset of lattice points can be extended to the Potts model. For instance, one can consider a Hamiltonian with a single strongly ferromagnetic bond, i.e., such that

$$\beta\mathcal{H} = -\beta \sum_{\langle \mathbf{x}\mathbf{y} \rangle} \delta(s_{\mathbf{x}}, s_{\mathbf{y}}) - (\beta' - \beta)\delta(s_{\mathbf{a}}, s_{\mathbf{b}}), \quad (57)$$

where $s_{\mathbf{a}}$ and $s_{\mathbf{b}}$ are the spins at the vertices of a lattice bond $\langle \mathbf{a}\mathbf{b} \rangle$. Here we set $\beta = \beta_c$ as we wish to investigate the behavior at the thermal FOT and consider $\beta' \neq \beta_c$. The equilibrium value of the energy in the FSS limit can be computed exactly, see App. B. Note that $0 < E_r < 1$ for any value of β' (even for a negative value), indicating that the system is always in the coexistence region. We can therefore apply the arguments of Sec. VIII. In Fig. 8

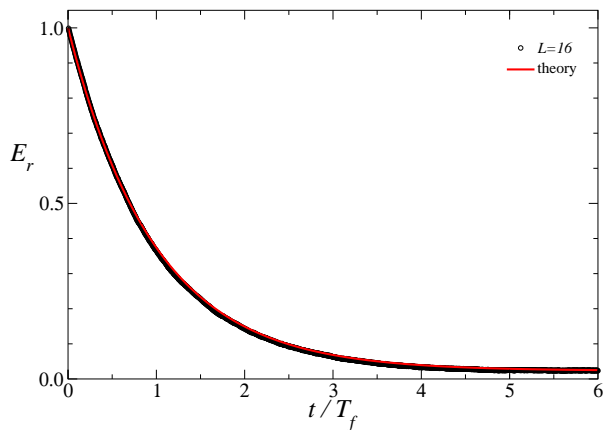


FIG. 8: (Color online) Renormalized energy $E_r(t)$ versus $t/T_f(0.1, L)$, where $T_f(0.1, L)$ is the first-passage time corresponding to $E_r = 0.1$. Simulation with $\beta' = 2\beta$ and $L = 16$. The thick line going through the points is the theoretical prediction.

we report numerical data for $\beta' = 2\beta_c$. Results scale as predicted by Eq. (50), provided we fix the ratio I_-/I_+ using the equilibrium value (B8).

XI. CONCLUSIONS

We have investigated the dynamic behavior of finite-size systems close to a FOT. Static quantities obey general FSS laws when expressed in terms of the scaling variable $r_1 = \delta L^d$, where d is the space dimension and δ specifies the distance from the transition point. At magnetic transitions we set $\delta = h$, where h is the magnetic field, while at thermal transitions one can take $\delta = \beta/\beta_c - 1$. If one considers the limit $\delta \rightarrow 0$ and $L \rightarrow \infty$ at fixed r_1 , one is always probing the coexistence region. Therefore, for periodic boundary conditions, or more generally for boundary conditions that do not favor a specific phase, the system oscillates among the different coexisting phases as the corresponding free energy barrier is finite. The relevant time scale $\tau(L)$ is the tunnelling time between the coexisting phases, which scales as $\tau(L) \sim L^\alpha \exp(\sigma L)$, where σ is proportional to the interface tension, and α is an appropriate exponent.

We develop a DFSS theory for the dynamic behavior in this regime, characterized by the coexistence of the two phases. If we consider time scales of the order of $\tau(L)$, the dynamic behavior can be described by using a two-state coarse-grained (Poisson) dynamics, that takes only into account in which phase the system is. This allows us to obtain exact predictions for the dynamical scaling functions.

The arguments that we present are general and therefore they should apply to any FOT with a discrete order parameter. Systems with continuous order parameters are expected to behave differently, because of the presence of Goldstone modes (see, e.g., Ref. [37], for a dis-

ussion).

We test these ideas in the 2D Ising and q -state Potts models. In the first case, we consider the magnetic FOTs that occur in the low-temperature phase for $h = 0$. We consider a purely relaxational dynamics at fixed h and T , starting from a completely ordered configuration. We investigate both the behavior for a uniform magnetic field and for a magnetic field that vanishes everywhere except on a lattice point or a lattice line. In the Potts case we set $q = 20$ and we consider the thermal FOT that is observed by varying the temperature. In particular, we consider the relaxational evolution using a heat-bath dynamics at fixed $T < T_c$, starting from a metastable disordered configuration. The numerical analyses for both models fully confirm the general picture.

Our study should be of particular relevance for experiments of moderately small systems (such as those we have considered for our tests), when the longest time scale of the system is of the order of the time scale of the experiment, as it may be the case in several physical contexts.

Appendix A: Ising model: Magnetization in the presence of a magnetic field on a single site

We compute here the magnetization for a finite system in which the magnetic field is non vanishing only at a single point (for definiteness we assume a finite h in the origin). If \mathcal{H}_0 is the Hamiltonian in the absence of a magnetic field and $\langle \cdot \rangle_0$ is the average with respect to \mathcal{H}_0 , we rewrite

$$\langle A \rangle_h = \frac{\langle A e^{\beta h s_0} \rangle_0}{\langle e^{\beta h s_0} \rangle_0}, \quad (\text{A1})$$

where A is an arbitrary function of the spins. Then, we use the identity

$$e^{\beta h s_0} = \cosh \beta h + s_0 \sinh \beta h, \quad (\text{A2})$$

which follows from the fact that s_0 takes only the values ± 1 . In the absence of a magnetic field $\langle s_0 \rangle_0$ vanishes and therefore we obtain

$$\langle A \rangle_h = \langle A \rangle_0 + \langle A s_0 \rangle_0 \tanh \beta h, \quad (\text{A3})$$

for any operator A . For the magnetization it follows

$$m(h) = \left\langle s_0 \left(\frac{1}{V} \sum_i s_i \right) \right\rangle_0 \tanh \beta h. \quad (\text{A4})$$

Using translation invariance we can rewrite

$$m(h) = \left\langle \left(\frac{1}{V} \sum_i s_i \right)^2 \right\rangle_0 \tanh \beta h. \quad (\text{A5})$$

In the absence of a magnetic field the average value is equal to m_0^2 and therefore

$$m(h) = m_0^2 \tanh \beta h. \quad (\text{A6})$$

Appendix B: Potts model: energy in the presence of an additional single-site bond energy term

In analogy with the Ising case we now compute the energy for a Potts model in which there is an additional energy term associated with a single bond. More precisely, if H_0 is the Potts Hamiltonian (41), we consider

$$\mathcal{H} = H_0 - a\delta(s_a, s_b), \quad (\text{B1})$$

where s_a and s_b are the colors at the vertices of an arbitrary lattice bond. If $\Delta\beta = \beta a$, and $\langle \cdot \rangle$ and $\langle \cdot \rangle_0$ are the averages with respect to Hamiltonians \mathcal{H} and H_0 , respectively, we have

$$\langle H_0 \rangle = \frac{\langle H_0 e^{\Delta\beta\delta(s_a, s_b)} \rangle_0}{\langle e^{\Delta\beta\delta(s_a, s_b)} \rangle_0}. \quad (\text{B2})$$

Now, since $\delta(s_a, s_b)$ takes only two values, 0 and 1, we can write

$$e^{\Delta\beta\delta(s_a, s_b)} = 1 + 2f\delta(s_a, s_b) \quad f = \frac{1}{2}(e^{\Delta\beta} - 1). \quad (\text{B3})$$

Using also the translational invariance of the model with Hamiltonian H_0 (we assume periodic boundary conditions), it follows

$$\langle H_0 \rangle = \frac{\langle H_0 \rangle_0 - f\langle H_0^2 \rangle_0/L^2}{1 - f\langle H_0 \rangle_0/L^2}. \quad (\text{B4})$$

If $E = \langle H_0 \rangle / L^2$ is the energy density for $a = 0$, we use the identity

$$\langle H_0^2 \rangle_0 = L^4 E^2 - L^2 \frac{\partial E}{\partial \beta}, \quad (\text{B5})$$

and Eq. (45) to derive at the critical point

$$\frac{1}{L^4} \langle H_0^2 \rangle_0 = \frac{(E_c^+)^2 + q(E_c^-)^2}{1 + q}. \quad (\text{B6})$$

If we define

$$E_r = \Delta_c^{-1} (\langle H_0 \rangle / L^2 - E_c^-), \quad (\text{B7})$$

we obtain

$$E_r = \frac{1 - E_c^+ f}{1 - E_c^+ f + q(1 - E_c^- f)}. \quad (\text{B8})$$

Note that $f \geq -1/2$ ($f = -1/2$ is obtained for $a \rightarrow -\infty$) and $E_c^\pm > -2$, so that E_r satisfies the strict inequality $0 < E_r < 1$.

-
- [1] M. E. Fisher and M. N. Barber, Scaling theory for finite-size effects in the critical region, *Phys. Rev. Lett.* **28**, 1516 (1972).
 - [2] M. N. Barber, Finite-size scaling, in *Phase Transitions and Critical Phenomena*, edited by C. Domb and J. L. Lebowitz (Academic Press, New York, 1983), Vol. 8.
 - [3] J. Cardy, *Finite-Size Scaling*, North Holland, Amsterdam, 1988.
 - [4] V. Privman ed., *Finite Size Scaling and Numerical Simulation of Statistical Systems* (World Scientific, Singapore, 1990).
 - [5] V. Privman, P. C. Hohenberg, and A. Aharony, Universal critical-point amplitude relations, in *Phase Transitions and Critical Phenomena*, Vol. 14, edited by C. Domb and J. L. Lebowitz (Academic Press, New York, 1991).
 - [6] A. Pelissetto and E. Vicari, Critical phenomena and renormalization-group theory, *Phys. Rep.* **368**, 549 (2002).
 - [7] M. Campostrini, A. Pelissetto, and E. Vicari, Finite-size scaling at quantum transitions, *Phys. Rev. B* **89**, 094516 (2014).
 - [8] P. C. Hohenberg and B. I. Halperin, Theory of dynamic critical phenomena, *Rev. Mod. Phys.* **49**, 435 (1977).
 - [9] P. Calabrese and A. Gambassi, Ageing Properties of Critical Systems, *J. Phys. A* **38**, R133 (2005).
 - [10] S. Gong, F. Zhong, X. Huang, and S. Fan, Finite-time scaling via linear driving, *New J. Phys.* **12**, 043036 (2010).
 - [11] B. Nienhuis and M. Nauenberg, First-Order Phase Transitions in Renormalization-Group Theory, *Phys. Rev. Lett.* **35**, 477 (1975).
 - [12] M.E. Fisher and A.N. Berker, Scaling for first-order phase transitions in thermodynamic and finite systems, *Phys. Rev. B* **26**, 2507 (1982).
 - [13] V. Privman and M. E. Fisher, Finite-size effects at first-order transitions, *J. Stat. Phys.* **33**, 385 (1983).
 - [14] M. E. Fisher and V. Privman, First-order transitions breaking $O(n)$ symmetry: Finite-size scaling, *Phys. Rev. B* **32**, 447 (1985).
 - [15] M.S.S. Challa, D.P. Landau, and K. Binder, Finite-size effects at temperature-driven first-order transitions, *Phys. Rev. B* **34**, 1841 (1986).
 - [16] K. Binder, Theory of first-order phase transitions, *Rep. Prog. Phys.* **50**, 783 (1987).
 - [17] C. Borgs and R. Kotecky, A rigorous theory of finite-size scaling at first-order phase transitions, *J. Stat. Phys.* **61**, 79 (1990).
 - [18] P. Calabrese, P. Parruccini, A. Pelissetto, and E. Vicari, Critical behavior of $O(N) \otimes O(2)$ symmetric models, *Phys. Rev. B* **70**, 174439 (2004).
 - [19] K. Vollmayr, J.D. Reger, M. Scheucher, and K. Binder, Finite Size Effects at Thermally-Driven First Order Transitions: A Phenomenological Theory of the Order Parameter Distribution, *Z. Phys. B* **91**, 113 (1993).
 - [20] M. Campostrini, J. Nespolo, A. Pelissetto, and E. Vicari, Finite-size scaling at first-order quantum transi-

- tions, Phys. Rev. Lett. **113**, 070402 (2014); Finite-size scaling at first-order quantum transitions of quantum Potts chains, Phys. Rev. E **91**, 052103 (2015).
- [21] A. Pelissetto and E. Vicari, Dynamic off-equilibrium transition in systems slowly driven across thermal first-order transitions, Phys. Rev. Lett. **118**, 030602 (2017).
- [22] N. Liang and F. Zhong, Renormalization-group theory for cooling first-order phase transition in Potts models, Phys. Rev. E **95**, 032124 (2017).
- [23] T. W. B. Kibble, Topology of cosmic domains and strings, J. Phys. A **9**, 1387 (1976).
- [24] W. H. Zurek, Cosmological experiments in superfluid helium?, Nature **317**, 505 (1985).
- [25] B. M. McCoy, Statistical Mechanics and Field Theory ed V V Bazhanov and C J Burden (Singapore: World Scientific, 1995)
- [26] R. K. P. Zia and T. E. Avron, Total surface energy and equilibrium shapes: Exact results for the $d = 2$ Ising crystal, Phys. Rev. B **25**, 2042 (1982) and references therein.
- [27] J. S. Langer, Theory of the condensation point, Ann. Phys. (NY) **41**, 108 (1967); Theory of nucleation rates, Phys. Rev. Lett. **21**, 973 (1968).
- [28] B. A. Berg, U. Hansmann, and T. Neuhaus, Simulation of an ensemble with varying magnetic field: A numerical determination of the order-order interface tension in the $D = 2$ Ising model, Phys. Rev. B **47**, 497 (1993).
- [29] A.J. Bray, Theory of phase-ordering kinetics, Adv. Phys. **43**, 357 (1994).
- [30] P. A. Rikvold, H. Tomita, S. Miyashita, and S. W. Sides, Metastable lifetimes in a inetic Ising model: Dependence on field and system size, Phys. Rev. E **49**, 5080 (1994) and references therein.
- [31] In the notations of Ref. [30], the nucleation time is proportional to $L^{-2}|h|^{-(b+c)} \exp(a/h)$. At fixed hL this allows us to predict $\alpha = b+c-2 \approx 0$, if we use the estimate $b+c \approx 2$ valid for the sequential update. For the random update, one expects $b+c = 3$ and correspondingly $\alpha = 1$.
- [32] R.J. Baxter, *Exactly solved models in statistical mechanics*, (Academic Press, 1982).
- [33] Several exact results are reported in F.Y. Wu, The Potts model, Rev. Mod. Phys. **64**, 235 (1982).
- [34] A. Billoire, T. Neuhaus, and B. A. Berg, A determination of interface free energies, Nucl. Phys. B **413**, 795 (1994).
- [35] C. Borgs and W. Janke, An explicit formula for the interface tension of the 2D Potts model, J Phys. I (France) **2**, 2011 (1992).
- [36] A. Tröster and K. Binder, Microcanonical determination of the interface tension of flat and curved interfaces from Monte Carlo simulations, J. Phys.: Condens. Matter **24**, 284107 (2012).
- [37] A. Pelissetto and E. Vicari, Off-equilibrium scaling behaviors driven by time-dependent external fields in three-dimensional $O(N)$ vector models, Phys. Rev. E **93**, 032141 (2016).